RSC Advances

PAPER

View Article Online
View Journal | View Issue

Cite this: *RSC Adv.*, 2017, **7**, 35346

One-pot synthesis of ethylbenzene/1-phenylethanol and γ-butyrolactone from simultaneous acetophenone hydrogenation and 1,4-butanediol dehydrogenation over copper based catalysts: effects of the support

Hari Prasad Reddy Kannapu, *[abc] Young-Woong Suh, *[bc] Anand Narani,[a] Veeralakshmi Vaddeboina,[a] David Raju Burri[a] and Rama Rao Kamaraju Seetha [a]

Received 17th May 2017
Accepted 10th July 2017

DOI: 10.1039/c7ra05558g

rsc.li/rsc-advances

The effect of the support in the simultaneous hydrogenation of acetophenone and dehydrogenation of 1,4-butanediol was studied using supported (MgO, γ-Al_2O_3, MgO–Al_2O_3 and SiO_2) copper (10 wt%) catalysts, prepared *via* impregnation. In this process, acetophenone was transformed to 1-phenylethanol/ethylbenzene and 1,4-butanediol converted to γ-butyrolactone/tetrahydrofuran under a hydrogen-free environment, indicating the major role of the supports. The Cu/MgO catalyst was active and highly selective towards the production of 1-phenylethanol and γ-butyrolactone. However, an adverse behaviour was observed over Cu/MgO–Al_2O_3. An extraordinary catalytic performance was obtained over Cu/SiO_2 with high selectivity for ethylbenzene (99%) and γ-butyrolactone (99%). Contrarily, no hydrogenation of acetophenone was observed over Cu/γ-Al_2O_3 due to the dehydration of 1,4-butanediol, yielding tetrahydrofuran. The main advantage of this process is that no external hydrogen is required for the hydrogenation of acetophenone. Copper dispersion, the reduction behaviour of copper, copper particle size and the acidity and basicity of the catalysts play important roles in the activity. All four catalysts were characterized using BET surface area, N_2O pulse chemisorption, XRD, XRF, H_2-TPR, XPS, and TPD of NH_3/CO_2 to understand our results.

1. Introduction

Biomass is one of the most important sources for the production of chemicals and fuels.[1] Lignin and cellulose are the chief source for the production of acetophenone (ACP)[2] and 1,4-butanediol (BDO),[3] respectively, which are potentially key platform molecules for the synthesis of value added chemicals. Hydrogenation of ACP can produce 1-phenylethanol (PhE), and ethylbenzene (EB), whereas BDO cyclodehydrogenation can form γ-butyrolactone (GBL) and its cyclodehydration can generate tetrahydrofuran (THF). PhE is industrially employed for making perfumery products[4–7] whereas EB is an important starting material in the manufacturing of styrene.[7] Because of the wider utility of both PhE and EB, intensive research has been conducted on the selective hydrogenation of ACP using supported noble metal catalysts[8–15] and base metal catalysts such as nickel[16–22] and copper[23] using harsh reaction conditions such as high temperatures and high hydrogen pressures in different solvents. However, the selective formation of PhE/EB is a highly challenging task in the current research. There is a possibility of getting 100% selectivity towards PhE/EB, but high hydrogen pressures and solvents are mandatory[8–23] that makes the system very complicate, expensive and not eco-friendly. Hence, an alternative and hydrogen free hydrogenation process should be developed immediately.

γ-Butyrolactone (GBL), an important bio-mass derived product, has a great potential in the synthesis of *N*-vinyl-pyrrolidone, *N*-methylpyrrolidone, herbicides, and rubber additives and also use as a green solvent. GBL can be produced from 1,4-butanediol (BDO) through cyclodehydrogenation process.[24] Commercially, the major production route for GBL is gas-phase dehydrogenation of BDO over supported copper metal catalysts, especially copper chromite catalysts, which are not environmentally friendly. At the same time tetrahydrofuran (THF) can be synthesized from BDO by employing acid catalyse systems *via* dehydration.[25–29] The enormous importance of these chemicals, due to derive from biomass, BDO conversion has received great attention.

[a]*Catalysis Laboratory, I&PC Division, Indian Institute of Chemical Technology, Hyderabad-500007, India. E-mail: kannapuhari@gmail.com*

[b]*Department of Chemical Engineering, Hanyang University, Seoul 133-791, Republic of Korea. E-mail: ywsuh@hanyang.ac.kr; Fax: +82-2298-4101; Tel: +82-2220-4329*

[c]*Research Institute of Industrial Science, Hanyang University, Seoul 133-791, Republic of Korea*

To minimize the severe reaction conditions and increases yield of PhE and EB from ACP hydrogenation, coupling of hydrogenation and dehydrogenation can be a promising method. Of late, coupling process has great attention due to the hydrogen economy, energy saving, operational simplicity and eco-friendly nature.[30–43] Aiming at utilizing these privileges cyclohexanol dehydrogenation to cyclohexanone and furfural hydrogenation to furfuryl alcohol has been performed simultaneously using Cu–MgO and promoted Cu–MgO catalysts at atmospheric pressure[38,40,43] under hydrogen free process at lower temperature than that of independent reactions. Due to more advantages of its application, we are interested to work on nitrobenzene (NB) hydrogenation with BDO dehydrogenation where aniline and GBL selectively formed over copper based catalysts.[24] Moreover, coupling of nitrobenzene hydrogenation and cyclohexanol dehydrogenation was conducted over Cu/MgO–Al_2O_3, where selectivity of the aniline and cyclohexanone improved greatly compared to single reactions.[44] Based on above studies, upgrading of bio chemicals such as ACP and BDO *via* coupling process would be a promising method due to hydrogen free process over copper based catalysts. To the best of our knowledge, it would be a first report on this process. It is fact that individual hydrogenation of ACP and BDO dehydrogenations is favourable over both acidic and basic supported catalysts.[8–24] Thus, developing of a suitable catalyst for simultaneous hydrogenation of ACP hydrogenation and dehydrogenation of BDO could be a challenging task.

Herein, we reported ACP hydrogenation coupled with BDO dehydrogenation over various supported (MgO, Al_2O_3, MgO–Al_2O_3 and SiO_2) copper catalysts in order to figure out the controlling of the product selectivity under similar reaction conditions. Activity studies have been carried out systematically over Cu/MgO, Cu/Al_2O_3, Cu/MgO–Al_2O_3 and Cu/SiO_2 catalysts. Catalysts were well characterized by using BET surface area, XRD, XRF, N_2O pulse chemisorption, TPR, XPS, TPD of NH_3, TPD of CO_2 and TGA analysis.

2. Experimental

2.1. Preparation of support

γ-Al_2O_3 (surface area 280 $m^2\ g^{-1}$) and fumed silica (390 $m^2\ g^{-1}$) are obtained from commercial source (M/s. Sigma-Aldrich, AR grade, 99%). But supports MgO and MgO–Al_2O_3 are prepared as described by ours earlier reports.[4,44] Typically, MgO support was prepared by precipitation method, a required quantity of Mg $(NO_3)_2\cdots 6H_2O$ dissolved in de-ionised water then followed by precipitation with 10 wt% aq. solution of K_2CO_3 with pH of 9. After the complete precipitation, the obtained gel was separated by filtration subsequently washed with distilled water till the attainment of neutral pH. Subsequently, the sample was dried at 373 K for 12 h and calcined at 723 K for 5 h at a ramping rate of 5 K min^{-1}. The resulting white MgO powder is used as a support. For the preparation of MgO–Al_2O_3 mixed oxide catalyst, we prepared Mg–Al hydrotalcite as stated in one of our publications.[44] In a typical procedure, solution A containing 256 g of Mg $(NO_3)_2\cdot 6H_2O$ (1 mol.) and 185.7 g of Al $(NO_3)_3\cdot 9H_2O$ (0.5 mol.), with Mg/Al molar ratio of 2 was prepared. Solution B was prepared by dissolving 280 g of 50 wt% NaOH (140 g in 140 mL distilled water) and 100 g of Na_2CO_3 in 1000 mL distilled water. Here NaOH provides OH^- while Na_2CO_3 delivers CO_3^{-2} ions to form a hydrotalcite structure. In order to prepare the MgO–Al_2O_3 hydrotalcite, solution A was added to solution B under constant stirring while maintaining the pH in the range of 11–12. The resulting gel was transferred to an autoclave and allowed to crystallise at 333 K for 18 h. Then, the sample is filtered and washed several times with hot water until the pH reached to neutral which ensure the total removal of Na^+. The final sample was dried in an oven at 373 K for 12 h and then calcined at 723 K in air for 18 h in order to obtain the MgO–Al_2O_3 mixed oxide.

2.2. Catalysts preparation

A certain amount of copper (10 wt%) was deposited on the above mentioned supports. Typically, for Cu/MgO catalyst, a required quantity of aqueous nitrate solution of Cu $(NO_3)_2\cdot 3H_2O$ was added to MgO support. The resulting slurry was stirred well on hot plate until removing excess water then subsequently dried in an oven at 373 K for 12 h. The solid residue was crushed to fine particles, sieved <200 μm and finally calcined in air at 723 K for 5 h. Similar procedures were applied to the rest of the catalysts and designated as Cu/Al_2O_3, Cu/MgO–Al_2O_3 and Cu/SiO_2.

2.3. Catalysts characterization

Catalysts were characterized using different analytical technique. BET surface area of the catalysts was measured on an Autosorb Automated Gas Sorption System (M/s. Quantachrome, USA) with N_2 as adsorbate at liquid nitrogen temperature. X-ray powder diffraction (XRD) patterns were recorded on a Rigaku Miniflex (M/s. Rigaku Corporation, Japan). X-ray diffractometer using Ni filtered Cu Kα radiation (λ = 1.5406 Å) with a scan speed of 2° min^{-1} and a scan range of 10–80°at 30 kV and 50 mA. The copper content of the catalysts was measured using a Wavelength Dispersive S4-Pioneer X-ray Fluorescence spectroscope (M/s. Bruker, Germany). N_2O pulse chemisorption was carried out at 303 K on a homemade pulse reactor to evaluate the copper dispersion and particle size. Typically, about 100 mg of the catalyst was placed in a reactor of 8 mm i.d., and then the catalyst was first reduced under a hydrogen flow at 523 K for 3 h, and then pre-treated at 523 K for 1 h under helium gas flow subsequently cool down to 303 K under same helium flow. The outlet of the reactor was connected to a micro-thermal conductivity detector (TCD) equipped GC-17A (M/s. Shimadzu Instruments, Japan) through an automatic six-port valve (M/s. Valco Instruments U.S.A). After cooling the reactor to the required temperature, pulses of 10% N_2O (balanced He) were injected to the catalysts at room temperature through a 1 mL loop connected to the six-port valve until no further change in the intensity of the outlet N_2O (from GC-software), assuming N_2O : Cu stoichiometry of 1 : 2 and Cu metal cross sectional area of 6.8×10^{-20} m^2 Cu atom $^{-1}$.[24] Temperature programmed reduction (TPR) of the catalysts were generated on a homemade on-line quartz micro reactor interfaced to a thermal

conductivity detector (TCD) equipped with a gas chromatograph (Varian CP 3800 USA) and the profiles were recorded using GC software. A H_2/Ar (10 vol% of H_2 and balance Ar) mixture was used as the reducing gas while the catalyst (amount of each catalyst weight is 50 mg) was heated at a linear heating ramp of 10 K min^{-1} from 303 to 900 K. X-ray photoelectron spectroscopy results were recorded on a Kratos Axis 165 XPS Spectrometer, with Mg Kα radiation (1253.6 eV) for reduced (523 K for 3 h) catalysts. Temperature programmed desorption (TPD) of NH_3 was conducted using a 10% NH_3 in helium mixture on a homemade reactor for measuring the acid sites of the catalysts. In a typical experiment, about 100 mg of the catalyst was placed in a reactor of 8 mm i.d., followed by conducting pretreatment at 573 K for 2 h under helium flow. After that, the catalysts were reduced under hydrogen flow at 523 K for 3 h, and then reactor was cool down to 333 K in helium flow. The outlet of the reactor was connected to a micro-thermal conductivity detector (TCD) equipped GC-17A (M/s. Shimadzu Instruments, Japan) through an automatic six-port valve (M/s. Valco Instruments U.S.A). After cooling the reactor to the required temperature, pulses of 10% NH_3 (balance helium) were injected to samples at 333 K temperature through a 1 mL loop connected to the six-port valve until no further change in the intensity of the outlet NH_3 (from GC-software). In a similar procedure, the basicity of the catalysts was measured using 10% CO_2 balanced He. Thermal gravimetric analysis (TGA) of Cu/SiO_2 before and after the reaction was carried out using TGA/SDTA 851e thermal system (Mettler Toledo, Switzerland). During the analysis samples were heated under air from 300 K to 1100 K at a heating rate of 10 K min^{-1}.

2.4. Activity test

Catalytic activity of different supported copper catalysts was investigated in hydrogenation of ACP and dehydrogenation of BDO and coupling of both reactions. Firstly, ACP hydrogenation and BDO dehydrogenation reactions were performed separately in a fixed-bed tubular reactor (10 mm i.d., 300 mm long glass reactor) using 0.5 g catalyst under atmospheric pressure. In a typical procedure, the catalyst sample was diluted with quartz beads with an equal amount of catalyst and then packed at the centre of reactor between two quartz wool plugs. Since, the copper is sintered beyond 573 K, the catalysts reduction carried out at 553 K under H_2 at a flow rate of 40 mL min^{-1} for 3 h. For independent BDO transformation, the feed rate was 1 mL h^{-1} and nitrogen fed as a carrier gas at flow rate of 18 mL min^{-1}. In the case of separate ACP hydrogenation hydrogen was used as reducing gas. Finally, for coupling process, the mixture of reactants containing ACP and BDO (1 : 2 mole ratio, feed = 1 mL h^{-1}) were injected in to the reactor using syringe pump (M/s. Secura FT, B. Braun Germany) under N_2 flow (18 mL min^{-1}). The above all experiments were conducted at weight hourly space velocity (WHSV) of 2 h^{-1}. The product mixture is collected every hour using an ice cold trap and analysed on a GC (GC-17A, M/s. Shimadzu instruments, Japan) using a Zebron ZB-WAX capillary column 0.53 mm in diameter and 30 m long.

3. Results and discussion

3.1. Catalysts characterizations

3.1.1. Physiochemical characterizations. The physicochemical properties and copper composition of all four catalysts are measured and tabulated in Table 1. As shown from the results, the BET surface area of supported copper catalysts is directly associated with the surface area of bare supports. The surface areas of bare supports MgO, γ-Al_2O_3, MgO–Al_2O_3 and SiO_2 are 40, 280, 65, 390 m^2 g^{-1}, respectively. Hence, the surface area of Cu/MgO is lowest whereas Cu/SiO_2 surface area is highest. In fact, the surface area of the catalysts can be attributed to the crystallinity of the supports. The surface area of mixed oxide supported copper catalyst *i.e.*, Cu/MgO–Al_2O_3 obtained between in the range of Cu/MgO and Cu/Al_2O_3 catalysts. The reason for decreasing in surface area of the catalysts is pore blocking of the supports by addition of copper.[4,43,44] The surface area is as follows in the increasing order Cu/MgO < Cu/MgO–Al_2O_3 < Cu/Al_2O_3 < Cu/SiO_2.

The amount of copper in all the catalysts determined by XRF is shown in Table 1, and it confirmed the copper composition of the catalysts is close to theoretical values (10 wt%). Copper dispersion (D_{Cu^0}) and particle size (P_{Cu^0}) calculated from N_2O pulse chemisorption are summarized in Table 1. The fundamental chemical equation between copper metal and N_2O is $2Cu + N_2O \rightarrow Cu_2O + N_2$. The distinct copper dispersion of catalysts indicates the role of supports as well as metal support interactions. As shown from the results, the copper dispersion increased from Cu/MgO–Al_2O_3 (4%) to Cu/SiO_2 (18%), revealed copper is highly dispersed over SiO_2 surface compared to all other supports. Though the Cu/MgO–Al_2O_3 catalyst has shown higher BET surface area than Cu/MgO, the copper dispersion of Cu/MgO–Al_2O_3 is lower (4%) than Cu/MgO catalyst (8 wt%),

Table 1 Physicochemical characterization of various supported copper catalysts[a]

Catalyst	Cu (wt%) from XRF	SA (m^2 g^{-1})	D_{Cu^0} (%)	P_{Cu^0}[b] (nm) reduced	P_{Cu^0}[c] (nm) reduced	P_{Cu^0}[c,d] (nm) spent
Cu/MgO	10.2	32	08	45	33	38
Cu/Al_2O_3	9.98	158	13	20	25	36
Cu/MgO–Al_2O_3	9.58	48	04	33	23	30
Cu/SiO_2	10.3	300	18	15	20	22 (24)[e]

[a] SA specific surface area, D_{Cu^0} Dispersion, P_{Cu} particle size from. [b] N_2O pulse chemisorption. [c] XRD. [d] After coupling reaction. [e] After time on stream study for 5 h.

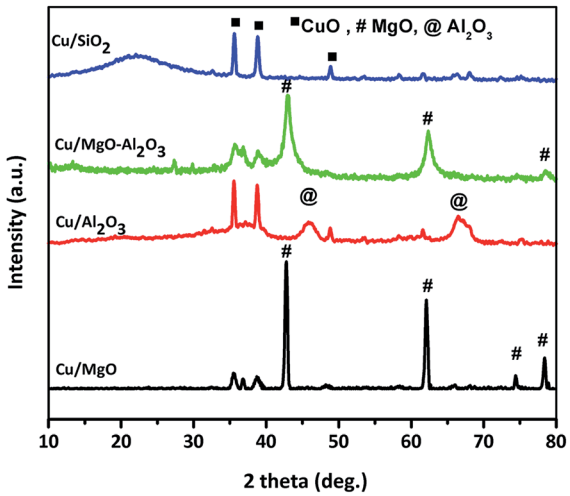

Fig. 1 X-ray diffraction studies of calcined supported copper catalyst.

probably due to incomplete reduction of copper oxide (discussed in TPR section). Apparently, the dispersion of copper in catalysts prepared by impregnation is affected by the calcination. The thermal treatment of the catalyst is accompanied by nucleation of new copper species. Depending on the structure of these species and the interaction with the support, nucleation will give rise to different metal dispersions.[45]

3.1.2. X-ray diffraction studies (XRD). The crystalline phases of calcined catalysts were confirmed by X-ray diffraction studies as shown in Fig. 1. The four supported copper catalysts exhibited characteristic peaks corresponding to CuO at 2θ 35.5, 38.7 and 48.5° (ASTM card no. 48-1548). The diffraction peaks appeared at 2θ 43.6°, 62.2°, 74.5° and 78.5°, corresponding to the MgO phase (ASTM card no. 04–829) were seen in both Cu/MgO and Cu/MgO–Al_2O_3 catalysts. Since, the alumina incorporation in to the MgO lattice a slight deviation towards higher 2θ can be noticed in MgO diffractions of mixed oxide catalyst. However, no MgO–Al_2O_3 hydrotalcite structure is observed, confirming the mixed-oxide formation after calcination.

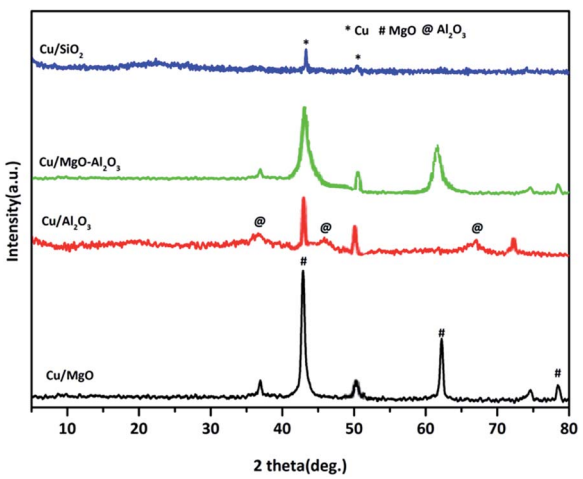

Fig. 2 X-ray diffraction studies of reduced supported copper catalyst.

Diffraction peaks at 2θ 36.8, 46.14 and 67.5°, assigned to Al_2O_3 phase were observed in the Cu/Al_2O_3 but they did not appear in the Cu/MgO–Al_2O_3 catalyst. The poor diffractions of γ-Al_2O_3 in Cu/MgO–Al_2O_3 and SiO_2 in Cu/SiO_2 confirmed the amorphous nature of both supports.[45,46] Interestingly, CuO diffractions in Cu/SiO_2 and Cu/Al_2O_3 seem to be sharp and higher intensity compared to other catalysts. The calculated crystallite size of copper oxide in MgO, Al_2O_3, MgO–Al_2O_3, SiO_2 is 55, 30, 38 and 16 nm, respectively.

XRD patterns of reduced copper catalysts are shown in Fig. 2. The typical characteristic diffractions at $2\theta = 43.29$, 50.5 and 74.5°, corresponding to Cu^0 indicated the complete reduction of CuO to Cu^0 metal in all the catalysts.

As shown in the Cu/MgO and Cu/MgO–Al_2O_3, the 100% Cu^0 plane (111) and 100% MgO plane (200) are not well separate due to the same 2θ.[4,43,44] But, alumina supported copper catalyst provided a well resolved copper diffractions. Contrarily, a poor diffraction peaks at 2θ of 43.29° and 50.5° corresponding to the copper metal were visible in Cu/SiO_2 catalysts, probably Cu^0 species presented in amorphous phase. Hence, the crystallite size of copper metal calculated using Debye–Scherrer formula for reduced catalysts is mainly based on copper plane (200) appeared at 2θ of 50.5° for all supported copper catalysts and the distinct crystallite size of copper can be seen in the Table 1. It was found that the study on SiO_2, Al_2O_3 and SiO_2–Al_2O_3 supported copper catalysts exhibited different crystallinity of copper metal which could be attributed to the interactions of copper and supports.[38,45,46] In addition to that, among all the supported copper catalysts silica supported copper catalyst displayed a smaller crystallinity of copper than the other catalysts mainly due to high dispersion of copper. This observation is quite resembled to Cu/SiO_2 in the present study, containing 18% copper dispersion with the mean crystallite size of 15 nm. In the case of spent catalysts after the coupling process the crystallite size of copper increased significantly due to agglomeration of copper.

The average Cu particle sizes from N_2O pulse chemisorption and crystallite sizes from XRD analysis of reduced catalysts are not same. This is probably because of the fact that the reduced catalysts while recording for their XRD are exposed to air and therefore, there is every possibility that some part of Cu^0 might be oxidized to Cu^{+1}/Cu^{+2}. The oxide copper species thus formed due to areal oxidation may be in the amorphous form. On the other hand an *in situ* reduction step was done at 523 K for 3 h prior to the N_2O pulse chemisorption. However, the trend of crystallite size follows the N_2O pulse chemisorption. Since our aim is to measure the Cu particle sizes, it is appropriate to use N_2O pulse chemisorption for the measurement of Cu particle sizes. This kind of phenomena was observed by Shohei *et al.*[47] where Ni/γ-Al_2O_3 catalysts provided different kinds of Ni particle sizes in XRD and N_2O pulse chemisorption studies. Nevertheless, it is worth noting that these techniques are agree generally well despite the very different physical principles involved (scattering effect *vs.* chemical titration).

3.1.3. Temperature programmed reduction (TPR). The reduction behaviour of different supported copper catalysts is investigated by temperature programmed reduction (TPR). The

TPR profiles of calcined catalysts are shown in the Fig. 3. It can be seen that the copper oxide reduction temperature is influenced by the support, confirming the existence of different metal-support interactions as well as various copper dispersions. The reason for step wise reduction of copper oxide over supported catalysts is still unclear. According to the literature, firstly CuO reduced to Cu_2O then reduced Cu_2O to Cu^0. It was also stated that surface CuO reduced at lower temperature whereas bulk CuO reduced at higher temperature. In the case of Cu/MgO catalyst, copper oxide reduced in two steps. The lower temperature reduction peaks including a shoulder peak at 600 K and 650 K were ascribed to the reduction of the surface copper species whereas a shoulder peak at 680 K was attributed to the reduction of residual bulk CuO. These results are well consistent with the literature.[48,49] In the case of Cu/Al_2O_3 catalyst, the reduction at 550 K with a shoulder peak at 580 K, corresponding to the surface and bulk copper oxide reduction was observed.

The TPR profile of Cu/SiO_2 catalyst had shown a single stage reduction with a shoulder at 620 K. The lower temperature hydrogen consumption at 550 K could be attributed to the reduction of surface copper oxides species whereas a shoulder peak at 620 K corresponding to the reduction of bulk copper oxides species. Remarkably, the copper oxide reduction at lower temperatures may indicate the high reduction ability of copper over alumina and silica supports.[46,48,49] By contrast, the TPR profile of $Cu/MgO–Al_2O_3$ catalyst is entirely different and exhibited two stage reduction at high temperatures compared to all other catalysts. The first hydrogen consumption peak at 670 K could be ascribed to the reduction of surface CuO whereas the second reduction at 800 K was attributed to the either reduction of interface copper oxide species or reduction of bulk CuO. Due to these unique interactions, copper might not reduce completely compared with that of other catalyst at 523 K, where all the catalysts were reduced for hydrogenation and dehydrogenation and coupling of both reactions. The amount of H_2 consumed, which can be determined from the peak area, corresponded to the amount of copper presented, *i.e.*, the H_2/CuO molar ratio was close to unity. The total hydrogen consumption estimated for Cu/MgO, $Cu/MgO–Al_2O_3$, Cu/Al_2O_3 and Cu/SiO_2 is 6.8 μmol g^{-1}, 4.2 μmol g^{-1}, 15.5 μmol g^{-1} and 20.8 μmol g^{-1}, respectively and the degree of copper reduction is as follows in the order of Cu/SiO_2 (95%) > Cu/Al_2O_3 (86%) > Cu/MgO (75%) > $Cu/MgO–Al_2O_3$ (59%). The results are associated with copper particle size of their catalysts. Moreover, TPR results are in accordance with N_2O pulse chemisorption results; since the lower copper dispersion of $Cu/MgO–Al_2O_3$ (4%) consumed smaller amount of hydrogen and higher copper dispersion of Cu/SiO_2 (18%) utilized higher hydrogen amount.

3.1.4. Temperature programmed desorption (TPD) of NH_3/CO_2. The acidic and basic properties of the catalysts play a vital role in the reaction path over supported metal catalysts. Acidic sites of reduced (523 K for 3 h) catalysts are determined by NH_3-TPD as shown in Fig. 4. The strength of acid sites is classified in to three types, such as weak acidic sites (423–573 K), medium acidic sites (573–773 K), and strong acidic sites (773–923 K). As shown from the result, two desorption peaks at 336 and 592 K with very low intensity, corresponding to weak and moderate acidic sites are noticed for Cu/MgO. Though MgO is a basic support, Cu/MgO catalyst contained a small amount of acidity. In the case of Cu/Al_2O_3, a broad desorption peak in the temperature range of 300–800 K was noticed, containing weak, moderate and strong acidic sites. Remarkably, $Cu/MgO–Al_2O_3$ catalyst provided a desorption peak at T_{max} of 643 K which reflect the moderate acid sites. In the case of Cu/SiO_2 catalyst two types of acidic sites in the temperature range of 300 K and 550 K were observed. The overall desorbed amount of NH_3 is quantified for each catalyst. The calculated NH_3 amount for Cu/MgO, Cu/Al_2O_3, $Cu/MgO–Al_2O_3$ and Cu/SiO_2 is 35 μmol g^{-1}, 816 μmol g^{-1}, 160 μmol g^{-1}, 203 μmol g^{-1}, respectively. Sun *et al.* reported that Cu/Al_2O_3 catalyst showed higher acidity compared with that of Cu/SiO_2.[46]

Basicity of reduced (523 K for 3 h) supported copper catalysts was determined by CO_2-TPD and profiles are shown in Fig. 5. The CO_2TPD profile of Cu/MgO displayed two strong CO_2 desorption at 650 and 850 K, indicating the presence of moderate and strong basic sites, which influenced on catalytic

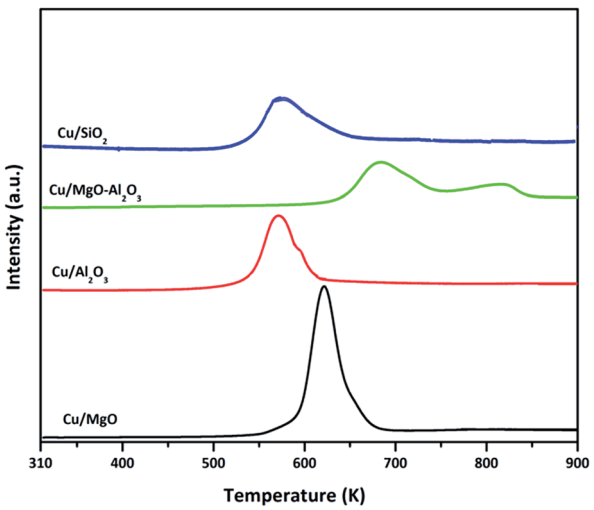

Fig. 3 TPR studies of calcined various supported copper catalyst.

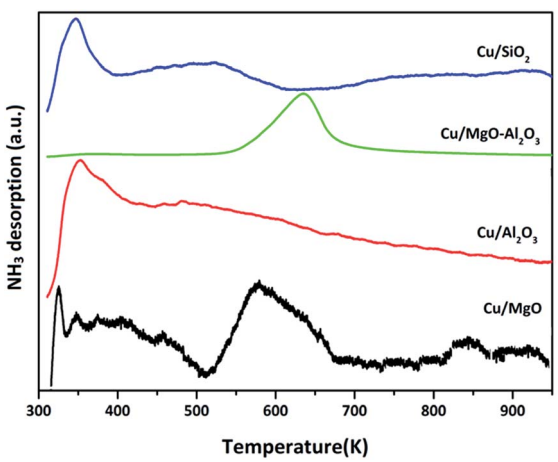

Fig. 4 NH_3-TPD patterns of various supported copper catalysts.

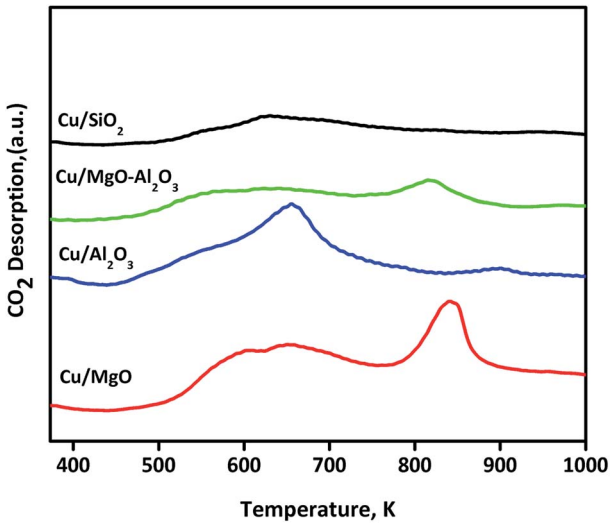

Fig. 5 CO_2-TPD patterns of various supported copper catalysts.

activity (discussed below). In the case of Cu/Al_2O_3, a single desorption at T_{max} of 650 K was ascribed to the moderate basic sites. Whereas, $Cu/MgO–Al_2O_3$ catalyst had two CO_2 desorption at a T_{max} of 643 and 850 K, corresponding to the moderate and strong basic sites, respectively. Contrarily, no strong desorption peak observed for Cu/SiO_2 catalyst. The basicity is as follows in the decreasing order: Cu/MgO 438 μmol g^{-1} > Cu/Al_2O_3 224 μmol g^{-1} > $Cu/MgO–Al_2O_3$ 180 μmol g^{-1} > Cu/SiO_2 45 μmol g^{-1}. These results are good accordance with literature reports.[46,48,49]

3.1.5. X-ray photoelectron spectroscopy (XPS). X-ray photoelectron spectroscopy (XPS) of reduced copper catalysts is shown in the Fig. 6. The XPS data provides more information about the copper oxidation state and particle size of the copper.

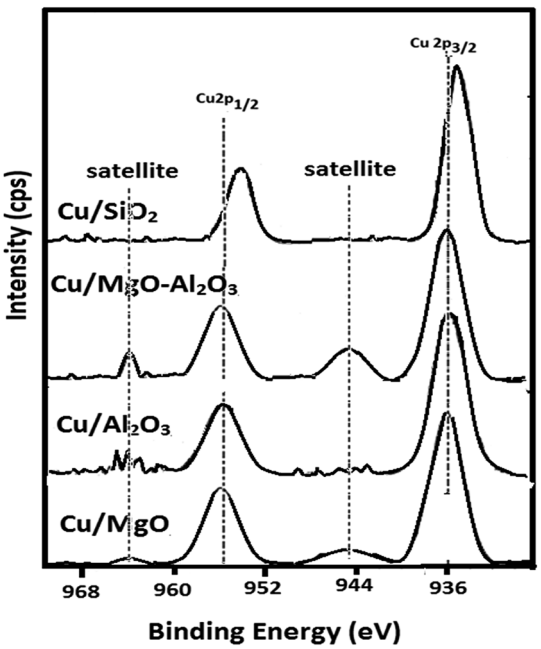

Fig. 6 XPS patterns of Cu of supported copper catalysts.

Table 2 Binding energy valves of Cu 2p and surface composition of Cu for different supported copper catalysts

Catalyst	Cu $2p_{3/2}$	Cu $2p_{1/2}$	Cu^0/support ratio
Cu/MgO	934.27	954.31	0.14
Cu/Al_2O_3	933.59	954.27	0.15
$Cu/MgO–Al_2O_3$	934.89	955.44	0.08
Cu/SiO_2	932.87	953.63	0.22

The binding energies of Cu $2p_{3/2}$ parent, Cu $2p_{1/2}$ peak and surface concentration of Cu to support are shown in Table 2. In general, satellite peaks indicates that copper presents in Cu^{+2} state and absence of satellite peak represents do not have Cu^{+2} species in the catalysts. Cu/MgO and $Cu/MgO–Al_2O_3$ both catalysts have satellite peaks centered at 944.35 eV and 944.38 eV, indicating incomplete reduction of CuO, probably due to bigger size copper particles as observed from N_2O pulse chemisorption (see, Table 1). But, Cu/Al_2O_3 and Cu/SiO_2 both have no satellite peak, confirming complete reduction of CuO to copper metal. The reduced samples are probably inferred to have two species Cu^+ and Cu^0 which is impossible to make a distinction between Cu^+ and Cu^0 on the basis of binding energy analysis alone.[38,39] The respective binding energy values of Cu in Cu/MgO, Cu/Al_2O_3 and $Cu/MgO–Al_2O_3$ related to the oxidation states of 0 to +1. Surprisingly, in the case of Cu/SiO_2 catalyst, the binding energy value of Cu $2p_{3/2}$ peak is very close to Cu^0 peak of bulk copper (not shown) and shifted to lower binding energy value than the other catalysts which could be attributed to the presence of more number of Cu^0 species on the Cu/SiO_2 catalyst surface. It is good accordance with N_2O pulse results (see, Table 1).

Furthermore, the XPS results demonstrated that the interactions between copper and supports may strongly influence on oxidation state of copper. Hence, the highly dispersed copper species did not re-oxidized whereas poorly dispersed or partially reduced copper metal species are yet again re-oxidized over the supports as the binding energy of copper in MgO and $MgO–Al_2O_3$ supported catalyst is high. In addition to that Cu^0/support ratio is high for Cu/SiO_2 and low for $Cu/MgO–Al_2O_3$ (See, Table 2).

3.2. Catalytic activity

Biomass is the chief source of lignin and cellulose, extraction of ACP from lignin[2] and BDO from cellulose[3] is well documented. Up gradation of biomass derived products has great attention in the chemical sector. As shown in Scheme 1, EB and GBL can be synthesised at a time from ACP and BDO, respectively. In another way, the *in situ* produced hydrogen from BDO dehydrogenation utilized in the hydrogenation of ACP for the production of EB *via* catalytic coupling of dehydrogenation and hydrogenation. The detailed catalytic activity study over different supported catalysts is as follows.

3.2.1. 1,4-butanediol (BDO) transformation over bare supports. Before examined the catalytic performance of all supported copper catalysts, controlled experiments were studied at 523 K over bare supports to examine the role of

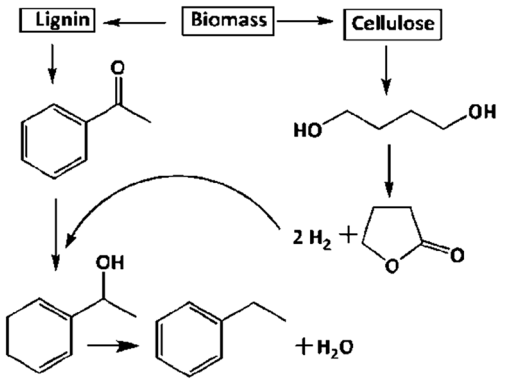

Scheme 1 Reductive upgrading of acetophenone (ACP) to ethylbenzene (EB) and 1,4-butanediol (BDO) to γ-butyrolactone (GBL) *via* coupling of simultaneous hydrogenation and dehydrogenation process.

Table 3 Catalytic activity of bare supports for ACP hydrogenation and BDO dehydrogenation[a]

Catalyst	Conv. of BDO (%)	Sel. of GBL (%)	Sel. of THF (%)	Conv. of ACP (%)	Sel. of EB (%)
MgO	Nil	Nil	Nil	2.8	100
Γ-Al_2O_3	60	Nil	>99	2.4	100
MgO–Al_2O_3	04	10	90	2.5	100
SiO_2	04	99	01	2.9	100

[a] Reaction conditions: catalyst = 0.5 g, T = 523 K, WHSV = 2 h^{-1}, BDO or ACP = 1 mL h^{-1}, N_2 or H_2 flow = 18 mL min^{-1}.

supports on BDO transformation and results are shown in Table 3. MgO support did not influence on BDO transformation, but γ-Al_2O_3 transforms BDO to THF with 60% conversion and >99% selectivity of THF. The mixed-oxide MgO–Al_2O_3 support transforms BDO to THF with 4% conversion and 90% selectivity of THF. Though SiO_2 is acidic support, conversion of BDO was <4% with 99% selectivity of GBL. Therefore, only supports did not have significant catalytic activity for the BDO to GBL in vapour phase.

3.2.2. Effect of temperature on BDO transformation. The catalytic activity of various supported copper catalysts has been studied for the transformation of BDO in temperature range from 473 to 573 K under nitrogen atmosphere using 0.5 g catalyst and results are shown in Fig. 7. The BDO conversion increased steadily with increasing the temperature up to 523 K, however beyond this temperature almost constant activity was noticed. BDO transformation is above 95% at 523 K over all catalysts except Cu/MgO–Al_2O_3 catalyst, indicating the optimum reaction temperature. In general, the enhancement in the BDO conversion with increase in temperature appraises the endothermic nature of BDO dehydrogenation.[4] Due to poor copper dispersion in Cu/MgO–Al_2O_3 catalyst, the catalytic activity is too low compared with other catalysts. In other words the stubborn reduction behaviour of copper on this support as shown in TPR may leads to lower activity though catalyst

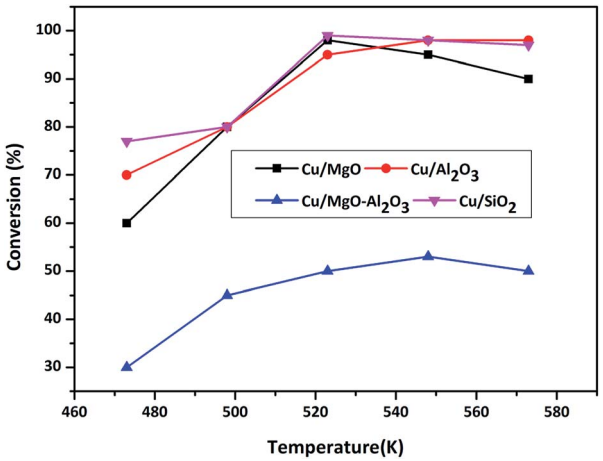

Fig. 7 Conversion of BDO as a function of temperature over different copper catalysts. Reaction conditions: catalyst = 0.5 g, WHSV = 2 h^{-1}, BDO feed flow = 1 mL h^{-1} and N_2 gas flow = 18 mL min^{-1}.

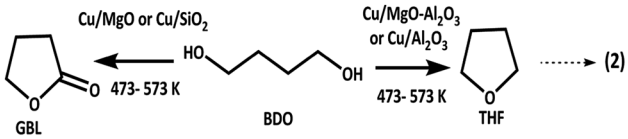

Scheme 2 BDO transformations over supported copper catalysts.

contained basic sites. As shown in the Scheme 2, BDO converts into products mainly in two different pathways, namely (i) dehydrogenation and (ii) dehydration.

Dehydrogenation of BDO transforms into GBL and H_2 whereas dehydration of BDO converts into THF and H_2O. Cu/MgO and Cu/SiO_2 catalysts produced GBL selectively (99%) from BDO *via* dehydrogenation, whereas Cu/MgO–Al_2O_3 and Cu/Al_2O_3 selectively produces THF (>90%) at all temperatures. According to Hwang *et al.*,[3] the Cu/SiO_2 is highly active for cyclodehydrogenation of BDO to GBL than dehydration of BDO to THF and results provided more than 99% BDO conversion with >99% selectivity of GBL and very low amount of THF (<1%) up to 5 h of time on stream study. Based on these findings, we assumed that the very weak Bronsted sites on silica might be involving in formation of low yield of THF. Al_2O_3 selectively catalyse the cyclization of BDO into THF at 548 K, because of its strong surface acidity. In addition, BDO is selectively dehydrated into THF over strong acid catalysts.[25–29] The influence of supported copper catalysts on dehydrogenation of BDO to GBL has been examined.[1,4,24,30] Since, the dehydrogenation of BDO to GBL is favourable over acid supported catalysts, it has been conducted over acidic supported catalysts such as Cu/Cr/Mn, Cu/Cr/Zn and Cu/Zn/Al. Moreover, Cu–Zn–Al was employed for hydrogenation of maleic anhydride and dehydrogenation of BDO and results obtained high yield of GBL. In the present study, Cu/SiO_2 and Cu/MgO catalysts are worked out well for this reaction.

In summary, weak to moderate acidic sites favours for the formation of GBL from BDO, whereas strong acidic sites

facilitates the formation of THF. Additionally, copper metal and the support interaction might also be responsible for the catalytic activity. The activity for BDO conversion to GBL is as follows in the increasing order Cu/Al_2O_3 < $Cu/MgO–Al_2O_3$ < Cu/MgO < Cu/SiO_2.

3.2.3. ACP hydrogenation

3.2.3.1. Effect of temperature on ACP hydrogenation. ACP hydrogenation was evaluated in the temperature range of 473–573 K under H_2 flow at atmospheric pressure over supported copper catalysts and results are shown in Fig. 8.

As shown in Scheme 3, hydrogenation of ACP can produces phE and EB. Before testing copper catalysts, effect of catalytic activity of bare supports on hydrogenation of ACP was also studied at 523 K under hydrogen and results are displayed in Table 3. Though the selectivity of EB is 100%, the conversion of ACP is <3%. Hence, the role of support is almost negligible on ACP hydrogenation reaction under the reaction conditions. When the reaction conducted over copper catalysts, the conversion of ACP is greatly improved. ACP conversion increases with the increasing of temperature up to 523 K but it decreased with further increasing in temperatures, which reflect the exothermic nature of ACP hydrogenation. Hydrogenation of ACP produced EB as a major product and PhE as a minor product. These results revealed that the conversion of ACP to EB is more favourable over Cu/SiO_2 (conv. 95%) and Cu/Al_2O_3 (conv. 80%) catalysts compared to Cu/MgO (conv. 48%) and $Cu/MgO–Al_2O_3$ (conv. 17%) catalysts at 523 K. Interestingly, the EB selectivity (99%) is not affected, even though different supported copper catalysts were employed.

Acidic supported catalysts have been examined for the hydrogenation of ACP and found that it is hard to get 100% selectivity of EB[8–23] without high hydrogen pressures. Moreover Ni and promoted Ni based catalysts had a poor selectivity towards EB due to higher activity of nickel for hydrogenation which gives over hydrogenated products like 1-cyclohexyl ethanol, cyclohexane and cyclohexene.[16–22] But, high ACP conversion with high

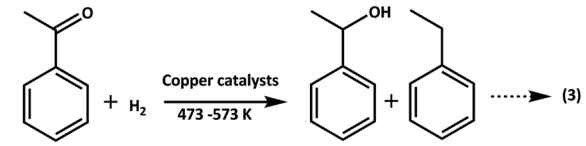

Scheme 3 ACP transformations over supported copper catalysts.

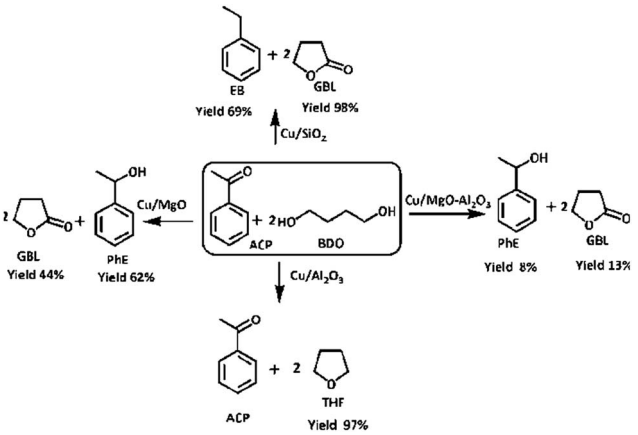

Scheme 4 Coupling of acetophenone hydrogenation and BDO dehydrogenation over supported copper catalysts.

EB selectivity was reported over heterogeneous copper based catalysts using high hydrogen pressure under solvents in liquid phase.[23] Noble metal catalysts such as Ru, Pd and Pt based catalysts showed high ACP conversion (80–90%) with 99% EB selectivity.[8–15] In the present study, Cu/SiO_2 surprisingly showed similar activity to that of noble metal catalysts. It is demonstrated that the smaller particle size of Cu^0 with higher dispersion as well as acidic nature of the catalyst are contributing for higher activity

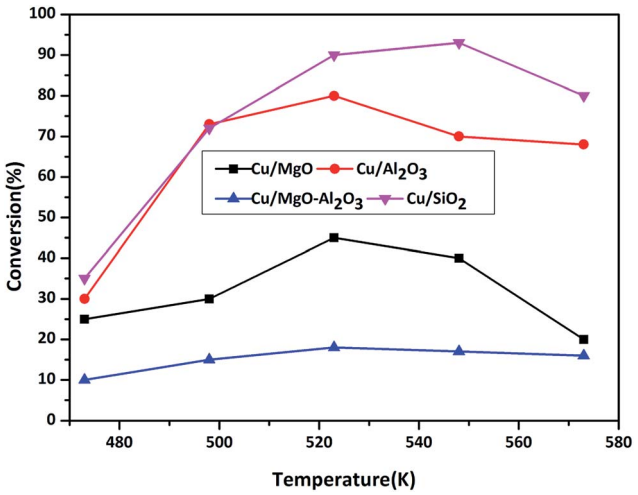

Fig. 8 ACP transformation as a function of temperature over supported copper catalysts. Reaction conditions: catalyst = 0.5 g, WHSV = 2 h^{-1}, ACP feed flow = 1 mL h^{-1} and H_2 gas flow = 18 mL min^{-1}.

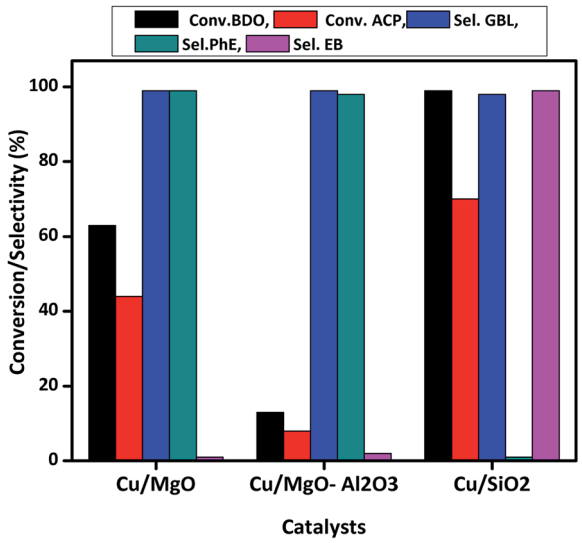

Fig. 9 Coupling of ACP hydrogenation and BDO dehydrogenation over supported copper catalysts at 523 K. Reaction conditions: catalyst = 0.5 g, WHSV = 2 h^{-1}, ACP and BDO mole ratio = 1 : 2, feed flow = 1 mL h^{-1} and N_2 flow = 18 mL min^{-1}.

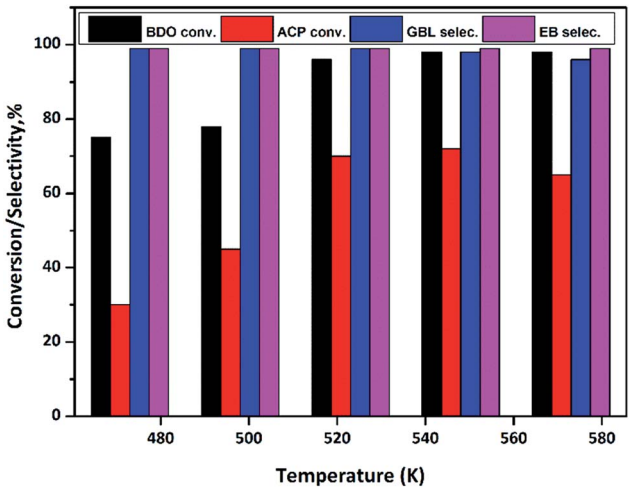

Fig. 10 Effect of temperatures on coupling of BDO dehydrogenation and ACP hydrogenation over Cu/SiO_2 catalyst. Reaction conditions: catalyst = 0.5 g, WHSV = 2 h^{-1}, temperature = 473–573 K, ACP and BDO mole ratio = 1 : 2, feed flow = 1 mL h^{-1} and N_2 flow = 18 mL min^{-1}.

compared to that of other supported catalysts. The activity is as follows in the decreasing order Cu/SiO_2 > Cu/Al_2O_3 > Cu/MgO > $Cu/MgO–Al_2O_3$.

3.2.4. Coupling of ACP hydrogenation and BDO dehydrogenation. According to Scheme 4, coupling of BDO dehydrogenation and ACP hydrogenation (2 : 1 mole ratios) reaction is carried out under N_2 flow (18 mL min^{-1}) in a fixed bed reactor over various supported copper catalysts at 523 K (optimum temperature obtained from individuals reactions) and results are shown in Fig. 9. The catalytic activity of Cu/Al_2O_3 in the coupling process for hydrogenation of ACP is negligible, because no hydrogen is produced from BDO, due to formation of THF.

Cu/MgO catalyst has shown better performance than $Cu/MgO–Al_2O_3$ in the present coupling process and selectively produced PhE (99%), no further hydrogenated products such as EB, cyclohexane and cyclohexene are observed due to its basic nature. XPS analysis of Cu/MgO catalyst found the two types of copper species (Cu^0/Cu^{+1}) on the MgO surface, resulting in less activity and high selectivity towards PhE. Though the selectivity of GBL and PhE are more or less equal to 99%, conversion of BDO and ACP are <10% over $Cu/MgO–Al_2O_3$ due to poor copper dispersion as observed from N_2O pulse chemisorption. The conversion of BDO and ACP are about 99% and 70%, respectively over Cu/SiO_2 catalyst with 99% selectivity of GBL and EB. It is clearly demonstrated that catalysts acidity played a vital role in the coupling process to make EB *via* hydrogenolysis of ACP in presence of copper. In addition to that, high copper dispersion over SiO_2 surface might enhances the hydrogenolysis of ACP.

In order to find out the optimum reaction temperature of the coupling process, a study is conducted over the temperature range from 473 to 573 K over Cu/SiO_2 catalyst and results are shown in Fig. 10. These results clearly show that conversion of BDO and ACP increases with increase in temperature from 473 to 523 K, however, further increasing in temperature no significant conversions observed in BDO. By contrast, ACP conversion decline at 573 K. In summary, to achieve the high conversions at lower temperature, the optimum reaction temperature seems to be 523 K.

Table 4 Coupling of BDO dehydrogenation and ACP hydrogenation over Cu/SiO_2 under different WHSV[a]

WHSV	Conv. of BDO (%)	Sel. of GBL (%)	Sel. of THF (%)	Conv. of ACP (%)	Sel. of EB (%)
1	99	99	1	73	99
2	98	99	1	70	99
3	50	99	1	40	99

[a] Reaction conditions: catalyst = 0.5 g, T = 523 K, WHSV = 2 h^{-1}, ACP/BDO mole ratio = 1 : 2, feed = 0.5,1 and 1.5 mL h^{-1}, N_2 flow = 18 mL min^{-1}.

Table 4 shows the WHSV test in the coupling process at 523 K over Cu/SiO_2 catalyst. As the increase of WHSV, the conversions of ACP and BDO are decreased. Interestingly, no significant changes are noticed in both conversions at WHSV of 1 and 2 h^{-1}. The catalytic performance of Cu/SiO_2 at WHSV of 3 h^{-1} is low, showing 50% and 40% of BDO and ACP conversions, respectively. However, the WHSV does not influence on the selectivities of GBL and EB. Hence, the optimum WHSV of coupling reaction is 2 h^{-1}.

Time-on-stream study is conducted at suitable reaction condition and results are displayed in Fig. 11. ACP and BDO conversions are 70% and 99%, respectively, with 99% selectivity of EB and GBL in the first hour. However, a gradual decrease in the conversion of both BDO and ACP is observed while the selectivities are constant. After confirming Cu/SiO_2 is the best catalyst for the coupling, ACP hydrogenation is conducted using

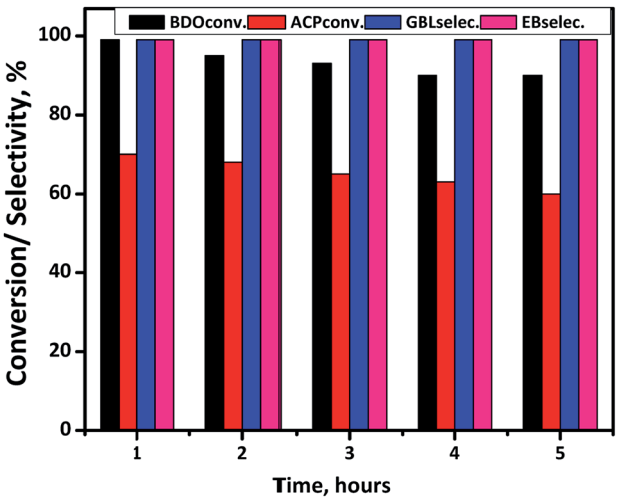

Fig. 11 Time-on-stream study for coupling of ACP hydrogenation and BDO dehydrogenation over Cu/SiO_2 catalyst at 523 K for 5 h. Reaction conditions: catalyst = 0.5 g, T = 523 K, WHSV = 2 h^{-1}, ACP/BDO mole ratio = 1 : 2, feed = 1 mL h^{-1} and N_2 flow = 18 mL min^{-1}.

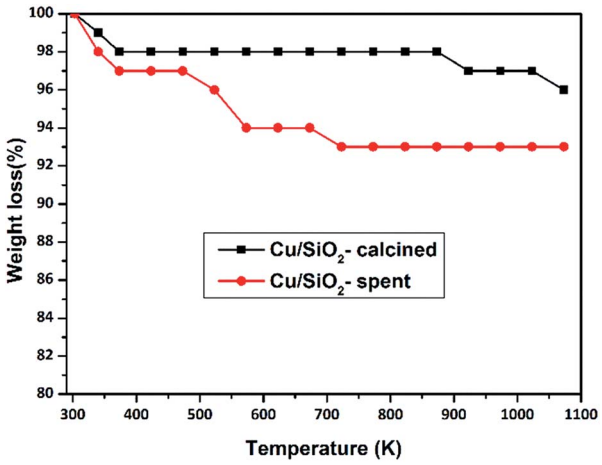

Fig. 12 TGA analysis of calcined and spent Cu/SiO_2 catalysts.

stoichiometric amount of external hydrogen and found the ACP conversion was <5%. Whereas in coupling process, the *in situ* produced hydrogen from BDO to GBL reaction substantially increased the conversion of ACP about 70%, indicating *in situ* generated H_2 is several times efficient than external hydrogen. The deactivation phenomena of this Cu/SiO_2 catalyst in gas-phase reactions is probably because of Cu sintering as shown in Table 1 at high reaction temperatures (523 K) as well as the partial oxidation of Cu^0 state. Besides that coke formation during the reaction is also influence the stability of the catalyst.

TGA analysis was used to investigate the formation of the coke and results of fresh and spent Cu/SiO_2 are shown in Fig. 12. In the case of fresh catalyst, an obvious mass loss was observed at 383 K, suggesting the removal of surface water molecules. However, no significant weight loss is occurred up to 950 K that may be due to decomposition residual amount of copper nitrate species. The spent catalyst weight loss around 390 K corresponds to the surface water molecules which is formed during the reaction. In addition to that two more weight loss are noticed at 550 K and 730 K, which confirms the coke formation due to the decomposition of either reactant or product or both of the molecules. Hence, this result confirms coke is another deactivation parameter to decrease the conversions of BDO and ACP in TOS study. The low temperature weight loss could be ascribed to the removal of easily oxidized carbon whereas another high temperature weight loss was the oxidation of regular or graphitic carbon. Hence, the stabilization of activity by suitable promoter is the future plan of this piece of work.

4. Conclusions

In summary, biomass-derived ACP and BDO are selectively converted to EB/1-PhE and GBL using copper based catalysts in a single reactor at a time *via* simultaneous hydrogenation and dehydrogenation. Among all catalysts, Cu/SiO_2 is found to be the best catalyst in terms of selective synthesis of GBL (98%) and EB (99%) whereas Cu/MgO has good performance for producing GBL (98%) and PhE (99%). The high selectivity of EB is probably because of acidic site along with more surface copper (Cu^0) atoms, which favours hydrogenolysis of ACP. But in the case of Cu/MgO, the strong basicity along with presence of copper species (Cu^0/Cu^{+1}) might be responsible for only selective formation of PhE. However, $Cu/\gamma\text{-}Al_2O_3$ is not active for coupling process, but highly active for individual hydrogenation and dehydration reactions due to its high acidity. Contrarily, the mixed-oxide supported $Cu/MgO–Al_2O_3$ catalyst has shown very poor catalytic activity due to its lower copper dispersion. Hence, the catalytic activity of the catalysts and reaction path can be influenced by both copper and support. The study presents several advantages (i) eco-friendly continuous process (ii) biomass to value added products (iii) conducting of both the reactions at a time, (iv) ACP hydrogenation without using H_2.

Acknowledgements

Authors are gratefully thanks to CSIR-UGC (INDIA) for the financial support. This research was also financially supported by Basic Science Research Program through the National Research Foundation of Korea (NRF) funded by the Ministry of Education (NRF-2016R1A6A1A03013422) and New & Renewable Energy Core Technology Program of the Korea Institute of Energy Technology Evaluation and Planning (KETEP), granted financial resource from the Ministry of Trade, Industry & Energy, Republic of Korea (No. 20143030091040).

Notes and references

1 H. P. R. Kannapu, C. A. Mullen, Y. Elkasabi and A. A. Boateng, *Fuel Process. Technol.*, 2015, **137**, 220–228.
2 C. Gonzalez, P. Marin, F. V. Diez and S. Ordonez, *Energy Fuels*, 2015, **29**, 8208–8215.
3 D. W. Hwang, P. Kashinathan, J. M. Lee, J. H. Lee, U.-H. Lee, J.-S. Hwang, Y. K. Wanga and J.-S. Chang, *Green Chem.*, 2011, **13**, 1672–1675.
4 K. Hari Prasad Reddy, N. Anand, V. Venkateswarulu, K. S. Rama Rao and B. David Raju, *J. Mol. Catal. A: Chem.*, 2012, **355**, 180–185.
5 E. H. Lee, *Catal. Rev.*, 1973, **8**, 285–305.
6 Y. Kashiwagi, K. Uchiyama, F. Kurashima, C. Kikuchi and J. Anzai, *Chem. Pharm. Bull.*, 1999, **47**, 1051–1052.
7 S. Liu, F. Chen, S. Xie, P. Zeng, X. Du and L. Xu, *J. Nat. Gas Chem.*, 2009, **18**, 21–24.
8 G. F. Santori, A. G. Moglioni, V. Vetere, G. Y. M. Iglesias, M. L. Casella and O. A. Ferretti, *Appl. Catal., A*, 2004, **269**, 215–223.
9 C. Chen, H. Chen and W. Cheng, *Appl. Catal., A*, 2003, **248**, 117–128.
10 L. Cerveny, Z. Belohlav and M. N. H. Hamed, *Res. Chem. Intermed.*, 1996, **22**, 15–22.
11 M. Casagrande, L. Storaro, A. Talon, M. Lenarda, R. Frattini, E. Rodrastellón and P. Maireles-Torres, *J. Mol. Catal. A: Chem.*, 2002, **188**, 133–139.
12 H. Cheng, J. Hao, H. Wang, C. Xi, X. Meng, S. Cai and F. Zhao, *J. Mol. Catal. A: Chem.*, 2007, **278**, 6–11.

13 M. A. Aramendía, V. Borau, J. F. Gómez, A. Herrera, C. Jiménez and J. M. Marinas, *J. Catal.*, 1993, **140**, 335–343.
14 A. Drelinkiewicza, A. Waksmundzka, W. Makowski, J. W. Sobczak, A. Król and A. Zieba, *Catal. Lett.*, 2004, **94**, 143–156.
15 S. D. Lin, D. K. Sanders and M. A. Vannice, *Appl. Catal., A*, 1994, **11**, 59–73.
16 J. Masson, S. Vidal, P. Cividino, P. Fouillox and J. Court, *Appl. Catal., A*, 1993, **99**, 147–159.
17 J. Masson, P. Cividino and J. Court, *Appl. Catal., A*, 1997, **161**, 191–197.
18 J. Masson, P. Cividino, J. M. Bonnier and P. Fouillox, *Stud. Surf. Sci. Catal.*, 1991, **59**, 245–252.
19 P. S. Kumbhar, *Appl. Catal., A*, 1993, **96**, 241–252.
20 J. M. Bonnier, J. Court and P. T. Wierzchowski, *Appl. Catal.*, 1989, **53**, 217–231.
21 R. V. Malyala, C. V. Rode, M. Arai, S. G. Hegde and R. V. Chaudhari, *Appl. Catal., A*, 2000, **193**, 71–86.
22 M. V. Rajashekharam, I. Bergault, P. Fouilloux, D. Schweich, H. Delmas and R. V. Chaudhari, *Catal. Today*, 1999, **48**, 83–92.
23 N. M. Bertero, C. R. Apesteguía and A. J. Marchi, *Appl. Catal., A*, 2008, **349**, 100–109.
24 K. Hari Prasad Reddy, R. Rahul, S. Sree Vardhan Reddy, B. David Raju and K. S. Rama Rao, *Catal. Commun.*, 2009, **10**, 879–883.
25 H. Inoue, S. Sato, R. Takahashi, Y. Izawa, H. Ohno and K. Takahashi, *Appl. Catal., A*, 2009, **352**, 66–73.
26 A. Igarashi, S. Sato, R. Takahashi, T. Sodesawa and M. Kobune, *Catal. Commun.*, 2007, **8**, 807–810.
27 N. Yamamoto, S. Sato, R. Takahashi and K. Inui, *Catal. Commun.*, 2005, **6**, 480–484.
28 N. Yamamoto, S. Sato, R. Takahashi and K. Inui, *J. Mol. Catal. A: Chem.*, 2006, **243**, 52–59.
29 S. Sato, R. Takahashi, T. Sodesawa and N. Honda, *J. Mol. Catal. A: Chem.*, 2004, **221**, 177–183.
30 Y.-L. Zhu, J. Yang, G.-Q. Dong, H.-Y. Zheng, H.-H. Zhang, H.-W. Xiang and Y.-W. Li, *Appl. Catal., B*, 2005, **57**, 183–190.
31 D. Zhang, H. Yin, R. Zhang, J. Xue and T. Jiang, *Catal. Lett.*, 2008, **122**, 176–182.
32 Y. Yu, Y. Guo, W. Zhan, Y. Guo, Y. Wang, Y. Wang, Z. Zhang and G. Lu, *J. Mol. Catal. A: Chem.*, 2011, **337**, 77–81.
33 M. Ueshima and Y. Shimasaki, *Catal. Lett.*, 1992, **15**, 405–411.
34 M. Glinski, *Appl. Catal., A*, 2008, **349**, 133–139.
35 R. Shi, F. Wang, X. Mu, Y. Li, X. Huang and W. Shen, *Catal. Commun.*, 2009, **11**, 306–309.
36 J. Yang, H.-Y. Zheng, Y.-L. Zhu, G.-W. Zhao, C.-H. Zhang, B.-T. Teng, H. Xiang and Y. Li, *Catal. Commun.*, 2004, **5**, 505–510.
37 H.-Y. Zheng, Y.-L. Zhu, L. Huang, Z.-Y. Zeng, H.-J. Wan and Y.-W. Li, *Catal. Commun.*, 2008, **9**, 342–348.
38 B. M. Nagaraja, A. H. Padmasri, P. Seetharamulu, K. Hari Prasad Reddy, B. David Raju and K. S. Rama Rao, *J. Mol. Catal. A: Chem.*, 2007, **278**, 29–37.
39 B. M. Nagaraja, A. H. Padmasri, B. David Raju and K. S. Rama Rao, *Int. J. Hydrogen Energy*, 2011, **36**, 3417–3425.
40 A. Malaika and M. Kozłowski, *Chem. Eng. J.*, 2011, **171**, 1348–1355.
41 Y. Saito, M. Yamashita, E. Ito and N. Meng, *Int. J. Hydrogen Energy*, 1994, **19**, 223–226.
42 B. M. Nagaraja, V. Siva Kumar, V. Shashikala, A. H. Padmasri, S. Sreevardhan Reddy, B. David Raju and K. S. Rama Rao, *J. Mol. Catal. A: Chem.*, 2004, **223**, 339–345.
43 C. V. Pramod, V. Mohan, B. David Raju and K. S. Rama Rao, *Catal. Lett.*, 2013, **143**, 432–437.
44 P. Sangeetha, K. Shanthi, K. S. Rama Rao, B. Viswanathan and P. Selvam, *Appl. Catal., A*, 2009, **353**, 160–165.
45 C. J. G. Van Der Grift, A. mulder and J. W. Geus, *Appl. Catal.*, 1990, **60**, 181–192.
46 W. Sun, D.-Y. Liu, H.-Y. Zhu, L. Shi and Q. Sun, *Catal. Commun.*, 2010, **12**, 147–150.
47 S. Tada, M. Yokoyama, R. Kikuchi, T. Haneda and H. Kameyama, *J. Phys. Chem. C*, 2013, **117**, 14652–14658.
48 Z. Yuan, J. Wang, L. Wang, W. Xie, P. Chen, Z. Hou and X. Zheng, *Bioresour. Technol.*, 2010, **101**, 7088–7092.
49 H. Yahiro, K. Murawaki, K. Saiki, T. Yamamoto and H. Yamaura, *Catal. Today*, 2007, **126**, 436–440.

